PHYSICAL REVIEW A **75**, 011403(R) (2007)

Alignment dynamics in a laser-produced plasma

C. Höhr, E. R. Peterson, N. Rohringer, J. Rudati, D. A. Arms, E. M. Dufresne, R. W. Dunford, D. L. Ederer, E. P. Kanter, B. Krässig, E. C. Landahl, R. Santra, S. H. Southworth, and L. Young

Argonne National Laboratory, Argonne, Illinois 60439, USA

(Received 26 July 2006; published 30 January 2007)

We observe the time evolution of ground-state ion alignment in a laser-produced plasma. Krypton ions produced in a strong, linearly polarized optical laser field (10^{14}–10^{15} W/cm^2) are aligned along the field polarization axis. Using microfocused, tunable x rays from Argonne's Advanced Photon Source, we measure orbital alignment as a function of time. For plasma densities of the order of 10^{14} cm^{-3}, the alignment decays within a few nanoseconds. A quantitative model explains the decay in terms of electron-ion collisions in the plasma. By applying an external magnetic field, we are able to suppress the disalignment and induce coherent spin precession of the Kr ions, thus providing an *in situ* monitor of magnetic fields in a plasma.

DOI: 10.1103/PhysRevA.75.011403 PACS number(s): 32.80.Rm, 33.35.+r, 52.20.Fs

Laser-produced plasmas have been objects of intense study due to their central role in the development of x-ray lasers [1,2], inertial confinement fusion [3], and advanced accelerator concepts [4]. In x-ray lasing schemes, laser-produced plasmas have been used as gain media whereby population inversion is achieved by electron-ion collisions or recombination followed by cascade [5]. Recently, laser-produced plasmas were used to amplify seed pulses from a high-order harmonic of a Ti:sapphire laser [6,7] and thus produce intense, ultrafast coherent radiation at ~32 nm. Typically, laser-produced plasmas are not in thermodynamic equilibrium and complex models are required to predict behavior, often with limited success [8]. It was suggested that tailored plasmas, suitable for recombination x-ray lasing schemes, could be achieved by tunnel ionization of gases [9]. Subsequently, plasmas produced by strong-field ionization of gaseous targets in the long-wavelength, long-pulse (10 μm, 500 ps) [10] and short wavelength, short-pulse (1–0.5 μm, sub-ps) [11] regimes were studied. Those experiments probed medium density plasmas (10^{18}/cm^3) using x-ray emission and optical Thomson scattering to characterize electron temperatures and showed qualitative, but limited quantitative, agreement with models. Of course, no information is obtained on ground state ion or neutral populations using emission methods. For such information absorption methods are required. In denser plasmas (10^{23}/cm^3) direct absorption using an "x-ray backlighter" continuum, generated by laser irradiation of a high-Z target, is feasible [8,12]. However, direct absorption methods are limited to dense targets where the plasma complexity prevents the extraction of individual state-to-state cross sections used in modeling.

Here we introduce the power of synchrotron-based x-ray microprobe methodology [13] to study dynamics in laser-produced plasmas. This versatile probe accesses ground states of ions. Moreover, the polarization and timing properties of the x rays and the plasma-generating laser provide the first access to ion alignment dynamics—with resolution at the 100 ps and 10 micron level. The brilliance of the synchrotron allows us to probe lower density plasmas (~10^{14}/cm^3), where dynamics are governed by isolated binary collisions. Thus, one can extract individual electron-ion scattering rate constants at eV energies, which are normally difficult to obtain because of the difficulty of producing ion targets with sufficient density [14]; such extracted cross sections provide benchmarks for advanced theoretical methods [15]. The synchrotron-based x-ray microprobe methodology is also readily scalable to the dense plasma regime.

We create a macroscopically aligned ensemble of Kr ions and demonstrate a resonance technique, analogous to NMR, to probe alignment dynamics in a transient plasma. Strong-field ionization of krypton gas by an ultrafast laser results in the coherent preparation of a collection of 10^7–10^9 Kr ions aligned along the laser polarization axis—which can be oriented either parallel or perpendicular to an external magnetic field. Specifically, the alignment is a population imbalance between the $m=\pm 1/2$ and $m=\pm 3/2$ magnetic sublevels of the $4p_{3/2}$ orbital hole formed in strong-field ionization of krypton [13]. We then monitor the dynamics of the aligned ion ensemble using resonant polarized x-ray absorption of the $1s \rightarrow 4p$ transition. The signature of alignment is a difference in the absorption strength for x-ray polarization parallel or perpendicular to the alignment axis. Our experiment is analogous to that of nuclear free-induction decay [16] where a pulsed rf field impulsively creates a large transverse magnetization and the return to equilibrium is observed in time using a pickup coil. Here the laser pulse plays the role of the rf pulse and the resonant polarized x-ray absorption is the "pickup coil" used to detect the alignment direction and magnitude as a function of time. In condensed matter systems, the spin relaxation is induced by random fluctuations within the spin-bath system. Here magnetic sublevel relaxation in Kr^+ is induced by collisions in our laser-produced plasma. We saturate single ionization of Kr with linearly polarized optical radiation to generate a single electron per Kr^+ ion and deplete the Kr neutral population. We start with nearly complete alignment, in contrast with previous plasma polarization studies where the degree of alignment, in excited states, is typically smaller and used to indicate anisotropic electron flow [17,18].

Alignment dynamics were studied under three conditions: no magnetic field, magnetic field parallel, and perpendicular to the Kr^+ alignment. Three axes are relevant: the alignment axis along the laser polarization $\hat{\epsilon}_L$, the x-ray polarization axis $\hat{\epsilon}_X$, and the magnetic field direction **B**. Creation of align-

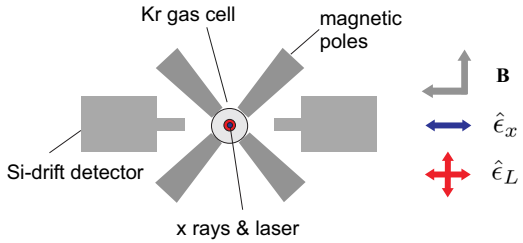

FIG. 1. (Color online) Experimental setup with magnetic field, laser, and x-ray orientations. X rays and laser copropagate into the plane of the page. For details see text.

ment was done with a Ti:sapphire laser (800 nm, 1 mJ/pulse, pulse length 65 fs) focused to 46 μm FWHM. Probing of the alignment was done with microfocused (6×7 μm FWHM), polarized x-ray pulses of 100 ps duration tuned to the Kr^+ $1s\rightarrow4p$ resonance at 14.312 keV. The x rays and laser beams were copropagated and spatially overlapped. The alignment was measured by delaying the x-ray probe pulse with respect to the laser pulse, for times up to 50 ns with a few ps precision. X-ray absorption was detected via the $K\alpha$ fluorescence with silicon drift detectors. The photon viewing region was limited to the central 1-mm section of the laser Rayleigh range. For the field-free case, we used an effusive gas jet target as described previously [13]. To apply an external magnetic field we used an electromagnet around an aluminum gas cell to impose either parallel or perpendicular **B** orientations (see Fig. 1). The target densities were estimated to 20% accuracy by combining the observed x-ray emission yields with known absorption cross sections [19], fluorescence decay branching ratios [20], the solid angle and efficiency for x-ray detection, and the incident x-ray flux.

First we discuss the alignment dynamics as a function of density in the absence of a magnetic field. In Fig. 2 we show the time development of the alignment at four plasma densities. At each density the resonant x-ray absorption is plotted for $\hat{\epsilon}_X$ parallel and perpendicular to $\hat{\epsilon}_L$, and are labeled $I_\parallel$ and $I_\perp$. Three qualitative features are readily apparent. At zero time delay, the $I_\parallel$:$I_\perp$ ratio is $\sim2:1$ for all densities—indicating almost complete alignment of the $4p_{3/2}$ orbital holes. (The x rays also resonantly excite $4p_{1/2}$ orbital holes which are unaligned.) This observed ratio agrees qualitatively with that expected from tunneling-ionization models [21,22] after inclusion of spin-orbit coupling effects [13,23]. Second, the $I_\parallel$ and $I_\perp$ curves merge at different times ($\sim2-20$ ns) for different target densities; the higher the density the faster the alignment decay. Third, there is an overall decay of the Kr^+ population that is roughly independent of the target density. This decay is due to the expansion of the localized plasma cloud which we observed by the appearance of the Kr^+ as a function of time outside the laser focal volume. We fitted an exponential decay to $I_\parallel+I_\perp$, and obtained a decay time $\tau=10\pm1$ ns for all target densities.

This observation implies that the electrons and their corresponding Kr^+ ions in the probed region expand together under these specific plasma conditions, i.e., $n_{\rm ion}(t)=n_{\rm el}(t)$, where $n_{\rm el}(t)$ and $n_{\rm ion}(t)$ are the electron and ion densities, respectively. Electrostatic arguments and the rather low elec-

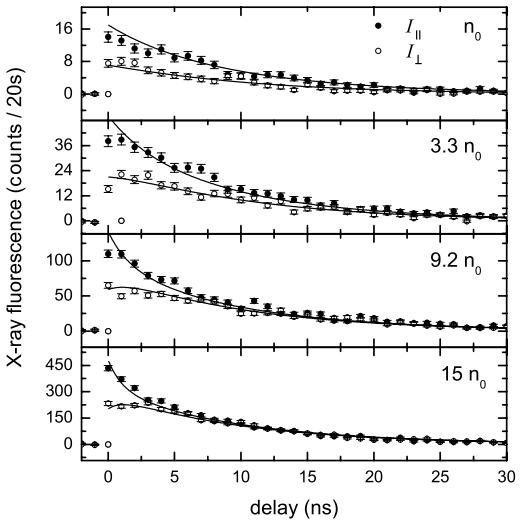

FIG. 2. Kr^+ orbital alignment decay for various densities. Kr^+ $1s\rightarrow4p$ resonance fluorescence versus laser/x-ray time delay for $\hat{\epsilon}_L$ and $\hat{\epsilon}_X$ parallel ($I_\parallel$) and perpendicular ($I_\perp$). Target density $n_0=1.3\times10^{14}$ cm^{-3}. Laser intensity is $1.0(0.2)\times10^{15}$ W/cm^2. Solid curves were generated by theory.

tron energies suggest that the laser-produced plasma remains quasineutral, reinforcing this assumption. In the laser focus, Kr^+ production is saturated. Hence, we set $n_{\rm ion}(0)$ equal to the target density. We define $\rho_{j,|m|}$ to be the fraction of Kr^+ in the angular momentum eigenstates $|j,\pm m\rangle$ and calculate using the quasistatic model the populations at $t=0$ generated by the laser pulse to be $\rho_{3/2,1/2}=69\%$, $\rho_{3/2,3/2}=5\%$, and $\rho_{1/2,1/2}=26\%$ [23].

The obvious candidate for causing relaxation amongst the magnetic sublevels is e^--Kr^+ collision. This leads to the following rate equations to describe the time evolution of the magnetic sublevels after the laser pulse

$$\dot{\rho}_i(t)=\sum_{i'\neq i}\{k_{i'\rightarrow i}\rho_{i'}(t)-k_{i\rightarrow i'}\rho_i(t)\}n_{\rm el}(t), \quad (1)$$

where $i\equiv j,|m|$. Knowing the time evolution of the $\rho_{j,|m|}$, the time-dependent x-ray absorption in the $\parallel$ and $\perp$ configurations can be calculated. Apart from an overall time- and $j,|m|$-independent factor, the x-ray absorption rates for the two configurations are given by

$$I_\parallel(t)=[2\rho_{1/2,1/2}(t)+4\rho_{3/2,1/2}(t)]n_{\rm ion}(t), \quad (2)$$

$$I_\perp(t)=[2\rho_{1/2,1/2}(t)+\rho_{3/2,1/2}(t)+3\rho_{3/2,3/2}(t)]n_{\rm ion}(t). \quad (3)$$

The factors multiplying the $\rho_{j,|m|}$ follow from angular momentum considerations [23]. Contributions from Kr^{++} and neutral Kr are neglected in Eqs. (2) and (3).

The six relevant transitions between the $|j,\pm m\rangle$ are shown in Table I. Experimental rate constants $k_{i\rightarrow i'}$ between magnetic sublevels were obtained by fixing the ratio of the rate constants between the $j=3/2\rightarrow3/2$, $3/2\rightarrow1/2$, and $1/2\rightarrow3/2$ transitions to their theoretical values and fitting simultaneously all the data shown in Fig. 2 to a single k. The values obtained from this fit procedure are listed in the second column of Table I.

TABLE I. Rate constants, in 10^{-7} cm^3 s^{-1}, for the electron-induced transition from the initial angular momentum state $|j_i,m_i\rangle$ (or $|j_i,-m_i\rangle$) of Kr^+4p^{-1} to the final states $|j_f,\pm m_f\rangle$.

$(j_i,m_i)\rightarrow(j_f,m_f)$	$k^{(\text{expt})}$	$k^{(\text{theory})}$
$\left(\frac{3}{2},\frac{1}{2}\right)\rightarrow\left(\frac{3}{2},\frac{3}{2}\right);\left(\frac{3}{2},\frac{3}{2}\right)\rightarrow\left(\frac{3}{2},\frac{1}{2}\right)$	1.08 (20)	1.37
$\left(\frac{3}{2},\frac{1}{2}\right)\rightarrow\left(\frac{1}{2},\frac{1}{2}\right);\left(\frac{3}{2},\frac{3}{2}\right)\rightarrow\left(\frac{1}{2},\frac{1}{2}\right)$	0.85 (14)	1.07
$\left(\frac{1}{2},\frac{1}{2}\right)\rightarrow\left(\frac{3}{2},\frac{1}{2}\right);\left(\frac{1}{2},\frac{1}{2}\right)\rightarrow\left(\frac{3}{2},\frac{3}{2}\right)$	1.36 (24)	1.72

We developed a theoretical model that quantitatively accounts for the observations. An electron scattering on Kr^+ $4p_{3/2}^{-1}$ sees a nonspherical charge distribution, with a leading quadrupole contribution in addition to the $-1/r$ potential. Magnetic interactions, e.g., spin-spin, are negligible in comparison to the electrostatic interactions considered here. The Hamiltonian of this simplified one-electron model is

$$\hat{H} = -\frac{1}{2}\nabla^2 - \frac{1}{r} - \frac{1}{r^3}\sqrt{\frac{4\pi}{5}}(\boldsymbol{Q}_2 \cdot \boldsymbol{Y}_2), \tag{4}$$

where $\boldsymbol{Q}_2$ is the atomic quadrupole tensor operator [24], $\boldsymbol{Y}_2$ is a spherical harmonic referring to the angular motion of the colliding electron, and $(\boldsymbol{Q}_2\cdot\boldsymbol{Y}_2)$ denotes the scalar product of the two spherical tensor operators. Utilizing a Herman-Skillman [25] potential, we estimate the quadrupole moment [24] of Kr^+ $4p_{3/2}^{-1}$ to be $Q=-1.4$ a.u. The cross section σ for a transition of Kr^+ from $|j_i,m_i\rangle$ to $|j_f,m_f\rangle$ is calculated using standard angular momentum algebra and employing a distorted wave Born approximation. That is, before and after the collision with the ionic quadrupole the electron is represented by a Coulomb wave. We average over the electron impact direction with respect to the ion alignment axis. This is motivated by the fact that Coulomb collisions with the ions and other electrons lead to rapid randomization of the electron motion after strong-field ionization.

To derive rate constants $k=\langle v\sigma\rangle$ we assume a classical model for the energy distribution of the photoelectrons [26], which is in reasonable agreement with observations [27]. For our laser parameters, the distribution is quasiexponential with a mean electron energy of $\bar{E}=2.98$ eV. The computed electron energy distribution and collision cross sections are used to calculate the rate constants $k=\langle v\sigma\rangle$ listed in the third column of Table I. The good agreement with the experimental data shown in Fig. 2 supports the electron-induced depolarization mechanism.

Next we discuss the alignment dynamics in the presence of a magnetic field. With all three axes—**B**, $\hat{\epsilon}_X$, $\hat{\epsilon}_L$—parallel to each other, a decay of the population is monitored in the time development of the x-ray absorption. The decay of alignment is then measured by orienting $\hat{\epsilon}_X$ orthogonally to **B** and $\hat{\epsilon}_L$. In Fig. 3 the upper and lower panels show the disalignment at low and high B fields, respectively [28]. Application of 410 G dramatically suppresses the decay of alignment. This is interesting because in studies of m-sublevel transfer in atom-atom collisions, B fields of 10 kG are required to substantially alter depolarization rates [29]. The obvious difference here is that an e^--ion collision is causing the m-sublevel transfer. Magnetic fields will have negligible effect on atom-atom trajectories, but can drastically alter the electron trajectories in the plasma. We believe that the external magnetic field imposes a post-laser interaction anisotropy on the overall electron trajectories which serves to preserve the alignment through cumulative collisions in the plasma. Note that at 400 G, the Kr^+ Zeeman splittings are of the order 10^{-5} eV and the cyclotron radius is ~ 10 μm. By contrast, the characteristic interaction energies during collisions are ~ 1 eV and the effective range of the depolarizing forces is only ~ 1 nm, so that individual electron-ion collisions are essentially unaffected by the magnetic field—unless the magnetic field leads to an overall reduced frequency of e^--Kr^+ close encounters.

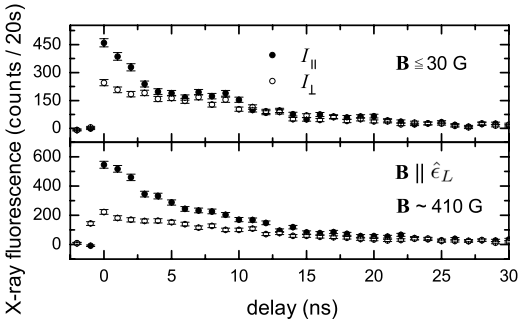

FIG. 3. Kr^+ $1s\rightarrow 4p$ resonance fluorescence as a function of laser/x-ray delay for low (<30 G) and high (410 G) magnetic fields. Target density, $n=2.3\times 10^{15}/\text{cm}^3$.

Finally, when the magnetic field is perpendicular to the alignment we have a situation analogous to pulsed NMR, where the aligned ions coherently precess around **B** at the Larmor frequency $\omega=g_j\mu_B B$. With the x rays polarized in the alignment direction, the resonant absorption will oscillate at 2ω [30]. The oscillation is seen in the top panel of Fig. 4. The Fourier transform (lower panel) yields the oscillation

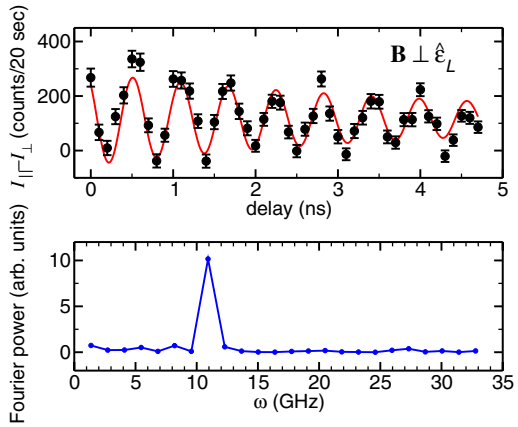

FIG. 4. (Color online) Top: Differential x-ray absorption $(I_\parallel - I_\perp)$ as a function of time delay for $\mathbf{B}\perp\hat{\epsilon}_L$. Bottom: Fourier transform of $(I_\parallel - I_\perp)$. Target density, $n=2.3\times 10^{15}/\text{cm}^3$.

frequency, 2ω which is an *in situ* measure of the local magnetic field. The line to guide the eye shown in the top panel is a cosine at the Fourier-determined frequency decaying with a ~5 ns time constant. Note that this decay time constant is much longer than that in bottom panel of Fig. 2 (~2 ns) measured at a similar target density with no **B** field.

In summary, we have introduced synchrotron-based x-ray microprobe methodology to probe dynamics of laser-produced plasmas with well-defined initial conditions. The methodology extends previous x-ray backlighter absorption methods to lower density plasmas where isolated binary collision models permit the extraction of electron-ion scattering rate constants at eV energies. Relative to backlighter methods, the addition of polarization control of both laser-pump and x-ray probe allows us to impulsively create and monitor an ensemble of aligned ions. We demonstrate control of alignment dynamics both through density and application of an external magnetic field. A simple theoretical model that includes the charge-quadrupole interaction in addition to the Coulomb potential for electron-ion collisions yields good agreement with the experimentally observed disalignment rates. Application of a magnetic field of 410 G dramatically prolongs the alignment. *In situ* magnetic field measurements are possible through the observation of Larmor precession. The combination of strong-field ionization with an x-ray microprobe provides an incisive tool to study polarization dynamics in a plasma.

This work was supported by the Chemical Sciences, Geosciences, and Biosciences Division and the Advanced Photon Source of the Office of Basic Energy Sciences, Office of Science, U.S. Department of Energy, under Contract No. W-31-109-ENG-38.

[1] M. M. Murnane *et al.*, Science **251**, 531 (1991).
[2] D. L. Matthews *et al.*, Phys. Rev. Lett. **54**, 110 (1985).
[3] J. Nuckolls *et al.*, Nature (London) **239**, 139 (1972).
[4] T. Tajima and J. M. Dawson, Phys. Rev. Lett. **43**, 267 (1979).
[5] H. Daido, Rep. Prog. Phys. **65**, 1513 (2002).
[6] Y. Wang *et al.*, Phys. Rev. Lett. **97**, 123901 (2006).
[7] Ph. Zeitoun *et al.*, Nature (London) **431**, 426 (2004).
[8] M. Fajardo *et al.*, Phys. Rev. Lett. **86**, 1231 (2001).
[9] N. H. Burnett and P. B. Corkum, J. Opt. Soc. Am. B **6**, 1195 (1989).
[10] W. P. Leemans *et al.*, Phys. Rev. Lett. **68**, 321 (1992); Phys. Rev. A **46**, 1091 (1992).
[11] T. E. Glover *et al.*, Phys. Rev. Lett. **73**, 78 (1994); Phys. Rev. E **57**, 982 (1998).
[12] P. Audebert *et al.*, Phys. Rev. Lett. **94**, 025004 (2005).
[13] L. Young *et al.*, Phys. Rev. Lett. **97**, 083601 (2006).
[14] I. D. Williams, Rep. Prog. Phys. **62**, 1431 (1999).
[15] K. Bartschat and I. Bray, J. Phys. B **30**, L109 (1997).
[16] E. L. Hahn, Phys. Rev. **77**, 297 (1950).
[17] T. Fujimoto and S. A. Kazantsev, Plasma Phys. Controlled Fusion **39**, 1267 (1997).
[18] J. C. Kieffer *et al.*, Phys. Rev. Lett. **68**, 480 (1992).
[19] S. J. Schaphorst *et al.*, Phys. Rev. A **47**, 1953 (1993).
[20] M. O. Krause, J. Phys. Chem. Ref. Data **8**, 307 (1979).
[21] M. V. Ammosov, N. B. Delone, and V. P. Krainov, Sov. Phys. JETP **64**, 1191 (1986).
[22] M. V. Frolov *et al.*, Phys. Rev. Lett. **91**, 053003 (2003).
[23] R. Santra, R. W. Dunford, and L. Young, Phys. Rev. A **74**, 043403 (2006).
[24] R. Santra and C. H. Greene, Phys. Rev. A **67**, 062713 (2003).
[25] F. Herman and S. Skillman, *Atomic Structure Calculations* (Prentice-Hall, Englewood Cliffs, NJ, 1963).
[26] P. B. Corkum, N. H. Burnett, and F. Brunel, Phys. Rev. Lett. **62**, 1259 (1989).
[27] J. L. Chaloupka *et al.*, Opt. Express **8**, 352 (2001).
[28] Residual fields in the pole pieces of ~30 G give rise to the small oscillations in the observed decay.
[29] J. C. Gay and W. B. Schneider, Phys. Rev. A **20**, 894 (1979).
[30] K. Blum, *Density Matrix Theory and Applications* (Plenum Press, New York, 1981), p. 155.